NJC

Accepted Manuscript

This is an *Accepted Manuscript*, which has been through the Royal Society of Chemistry peer review process and has been accepted for publication.

Accepted Manuscripts are published online shortly after acceptance, before technical editing, formatting and proof reading. Using this free service, authors can make their results available to the community, in citable form, before we publish the edited article. We will replace this *Accepted Manuscript* with the edited and formatted *Advance Article* as soon as it is available.

You can find more information about *Accepted Manuscripts* in the Information for Authors.

Please note that technical editing may introduce minor changes to the text and/or graphics, which may alter content. The journal's standard Terms & Conditions and the Ethical guidelines still apply. In no event shall the Royal Society of Chemistry be held responsible for any errors or omissions in this *Accepted Manuscript* or any consequences arising from the use of any information it contains.

ROYAL SOCIETY OF CHEMISTRY

www.rsc.org/njc

Journal Name

ARTICLE

Received 00th January 20xx,
Accepted 00th January 20xx
DOI: 10.1039/x0xx00000x
www.rsc.org/

Support Effects in Rare Earth Element Separation Using Diglycolamide-Functionalized Mesoporous Silica

Estelle Juère,[a,b] Justyna Florek,[a,b] Dominic Larivière,[a,c*] Kyoungsoo Kim[d] and Freddy Kleitz[a,b*]

Due to the rapidly increasing energy demand and growing production of high technology devices, the development of new sequestration materials for rare earth elements (REEs) has become critical. Nowadays, REEs play a predominate role as supplies for the transition to cleaner energy and production of economically important modern devices, such as wind turbines (Pr, Nd, Sm, Dy), car catalysts (Ce) or hybrid vehicles (Dy, La, Nd). However, for all these applications, only a very pure and isolated form of an element can be used. While several methods have been developed for REEs extraction, such as liquid-liquid (LLE) or liquid-solid extraction methods, the selective separation and purification of REEs still remain challenging. Industrially, the separation/purification process of REEs involves several liquid-liquid extraction (LLE) cycles. As a consequence, a large volume of solvents, time and labor is required. Moreover, LLE usually generates huge amount of wastes that are often environmentally harmful. Therefore, in our laboratories we have recently focused on developping greener alternatives for the REEs extraction process using solid extraction systems. In the present study, we use a tailored-made solid phase (SPE) extraction system, where properly modified mesoporous silica supports (i.e., SBA-15, SBA-16 and MCM-41) are used and compared as sorbents. As evidenced from our results, the DGA-functionalized porous sorbents are characterized by a pronounced selectivity towards mid-size elements and high stability in the extraction condition tested. Moreover, these sorbents possess very fast REEs uptake, being about 5 min. Further, we focus our studies on elucidating the influence of the pore structure, pore size and pore connectivity of the different silica materials on the static and dynamic extraction/purification of REEs.

Introduction

Owing to their unique properties, REEs became the strategic metals for advanced and green technologies. Lasers, wind turbines, hybrid cars, fluorescent lamps are only just a few representative examples of the broad range of REEs applications[1]. The global interest towards cleaner and coal-free technologies also significantly increased the overall market value of REEs. As a result, rare earth metals became essential materials for our economy and further industrial development. However, on-going intensive mining and lack of efficient REEs recycling strategy put these metals in a very critical place, where supplies drastically diminish while global needs increased[2]. Moreover, recent reduction in the REEs exportation from China rose the price of REEs and made mining prospection for these elements more compelling[3]. While China continued to occupy a dominant position in the REEs area, academics, industries and governments focused their research activities on the alternative sources for these critical elements[4]. Among different possibilities, the recovery of REEs from industrial wastes and end-of-life products represents an economically attractive and viable approach. However, similar properties of REEs make their separation and purification processes very tedious, demanding and environmentally unfriendly. For instance, the industrial recycling of REEs from the mining residues requires first a long treatment with huge amount of concentrated acids or bases[5]. In the second step, after adjustment of the pH of the mixture of REEs, the individual elements are separated by repeating several liquid-liquid extraction (LLE) steps. Alternatively, the solid-phase extraction (SPE) or supported liquid-liquid extraction (SLLE) can be used in this step; however, this process still suffers from many drawbacks, such as lack of selectivity of the ligand and leaching of the latter due to the

[a] Department of Chemistry, Université Laval, Québec, Canada G1V 0A6. E-mails: freddy.kleitz@chm.ulaval.ca; dominic.lariviere@chm.ulaval.ca; Fax: +1-418-656-7916; Tel: +1-418-656-7812.
[b] Centre de Recherche sur les Matériaux Avancés (CERMA), Université Laval, Québec, Canada G1V 0A6.
[c] Centre en Catalyse et Chimie Verte (C3V), Université Laval, Québec, Canada G1V 0A6.
[d] Center for Nanomaterials and Chemical Reactions, Institute for Basic Science (IBS), Daejeon 305-701, Korea.

Electronic Supplementary Information (ESI) available: Low angle XRD patterns of the materials. Additional HRSEM images. N_2 sorption isotherms of the pure silica materials and grafted SBA-16 material, PSD of all materials. IR spectra, mass loss profile and elemental analysis of the functionalized materials. Ln extraction (K_d) of the grafted SBA-15 materials. Linear regression and the corresponding parameters of the experimental data of the kinetic and the adsorption isotherm experiments. See DOI: 10.1039/x0xx00000x

non-chemically anchored ligand[6]. We believe that diglycolamide (DGA)-modified mesoporous silica sorbents can significantly improve the existing separation system by providing better separation factors and higher reusability potential[7]. Moreover, such a system lowers the solvent consumption needed for the separation, which in turn will reduce the separation costs. Nevertheless, more insights into the nature and role of the selected supports are still needed for optimization of the process, in particular regarding application under dynamic flow-through conditions. In the present contribution, we mainly focus our research on the investigation of the role of the silica support, its structure and its porosity on the extraction efficiency. To do so, we compare different silica materials, i.e., SBA-15, MCM-41 and SBA-16 solids of different pore sizes, functionalized with the same DGA-type ligand and tested these sorbents in the liquid-solid extraction system in both, static and dynamic extraction conditions.

Experimental section

Materials

Synthesis of the Ordered Mesoporous Silica

Mesoporous silica materials SBA-15 were synthesized according to the method reported by Choi et al.[8] 13.9 g of Pluronic P123, 252 g of distilled water and 7.7 g of HCl (37 %) were mixed at 35 °C under vigorous stirring. After the complete dissolution, 25 g of TEOS was added at once. This mixture was left at 35°C for 24h followed by the aging steps at various temperatures, i.e., at 60, 80, 100 or 130 °C for 24h under static conditions.

The cage-like mesoporous SBA-16 material was synthesized using the procedure reported by Kleitz et al.[9] 5 g of Pluronic F127 ($EO_{20}PO_{70}EO_{20}$, Sigma-Aldrich), 240 g of distilled water and 10.5 g of HCl (37 %) were mixed at 45 °C under vigorous stirring. After complete dissolution, 15 g of n-butanol was added. The mixture was left at 45 °C for 1h under stirring, after which 23.6 g of TEOS was added at once to the homogenous clear solution. The mixture was left at 45 °C for 24h under stirring followed by the aging step at 100 °C for 24h under static conditions.

The MCM-41 material was obtained following the method reported by Kleitz et al.[10] 9.65 g of cetyltrimethylammonium bromide CTAB ($CH_3(CH_2)_{15}N(Br)$-$(CH_3)_3$, Aldrich) was dissolved in 480 g of distilled water at 35 °C under stirring. After complete dissolution, 36.5 mL of NH_4OH (29%, Anachemia) was added. The temperature was reduced to 25 °C. After 15 min, 40 g of TEOS was added at once and the mixture was left for 2h under stirring, followed by an aging step at 90 °C for 3 days under static conditions.

For all synthetized materials, after the aging steps, the resulting white solids were filtered and dried at 100 °C for 24h. For the surfactant removal, the as-synthesized SBA-15 and SBA-16 materials were first slurried in the ethanol-HCl mixture, subsequently dried 24h at 100°C and finally calcined at 550 °C for 2h in air; the as-made MCM-41 material was directly calcined at 550°C for 5h.

The silica materials will further be cited as SBA-15(60), SBA-15(80), SBA-15(100), SBA-15(130) and SBA-16(100). Note that number in the parenthesis refers to the temperature of the aging treatment used during the synthesis of the SBA-15 and the SBA-16 type materials.

Ligand synthesis and anchoring on the silica support

The DGA ligand was synthetized as follows: 0.06 mL of diglycolyl chloride (DGACl, Sigma-Aldrich) was dissolved in 30 mL of anhydrous toluene (Sigma-Aldrich) under stirring and inert atmosphere (N_2 flow), with an ice bath. Then, 0.25 mL of (3-aminopropyl)triethoxysilane (APTS, Sigma-Aldrich) and catalytic amount of the triethylamine (TEA, Alfa Aesar, 99%) was added. The reaction was continued at room temperature for 24h under stirring and inert atmosphere. This mixture was further used without any purification steps. The structure of the modified silane was confirmed by ^{1}H NMR analysis: ($CDCl_3$) δ = 0.61 (Si-C<u>H</u>$_2$, 4H, t); 1.18 (C<u>H</u>$_3$-CH$_2$, 18H, t); 1.62 (CH$_2$-C<u>H</u>$_2$-CH$_2$, 4H, m); 3.27 (C<u>H</u>$_2$-NH, 4H, q); 3.78 (CH$_3$-C<u>H</u>$_2$, 12H, q); 3.99 (CO=C<u>H</u>$_2$-O, 4H, s); 6.78 (NH, br.) ppm.

The as-prepared mixture of modified silane was grafted on the silica surface in one step. Prior to the addition of the modified silane, 0.5 g of activated mesoporous silica (treated overnight at 150 °C under vacuum) was dispersed in 50 mL of anhydrous toluene. The mixture was refluxed at 110 °C for 2h under stirring and N_2 flow. Then, the modified silane solution was transferred and the resulting mixture was left at 110 °C for 24h under stirring and inert atmosphere. After cooling down the temperature to RT, the solid product was filtered, washed with toluene and ethanol three times and dried at 70 °C overnight in air. Soxhlet extraction was used to remove un-reacted silane molecules in dichloromethane for 6h. The final product was dried at 70 °C overnight in air.

Materials Characterization

N_2 adsorption-desorption isotherms were measured at -196 °C (77 K) using an Autosorb-iQ_2 sorption analyzer (Quantachrome Instruments, Boynton Beach, FL, USA). Prior to the measurements, the samples were outgassed at 200 °C for 10h, for the parent silica or at 80 °C for 12h, for the functionalized materials. The specific surface area (S_{BET}) was determined using the Brunauer-Emmet-Teller (BET) equation in the range $0.05 \le P_0 \le 0.2$ and the total pore volume (V_{pore}) was assessed at $P/P_0 = 0.95$. The pore size distributions were calculated from either desorption or adsorption branch using the non-local density functional theory (NLDFT) method considering the sorption of N_2 at -196 °C (77 K) in cylindrical pores for SBA-15[11] and MCM-41[12] samples or in the spherical pores for SBA-16[13] materials. Thermogravimetric analysis - Differential scanning calorimetry (TGA-DSC) measurements were performed using a Netzsch STA449C thermogravimetric analyzer, under air flow of 20 or 40 mL min^{-1} with a heating rate of 10°C min^{-1}. ^{13}C cross-polarization CP/MAS and ^{29}Si magic-angle-spinning (MAS) nuclear magnetic resonance (NMR) analyses were

carried out on a Bruker Advance 300 MHz spectrometer (Bruker Biospin Ltd, Milton, Ontario) at 75.4 MHz for ^{13}C and 59.6 MHz for ^{29}Si. ^{29}Si MAS NMR spectra were recorded with a spin echo sequence to avoid instrument background with a recycle delay of 30 seconds in a 4 mm rotor spin at 4 kHz. ^{13}C CP/MAS NMR spectra were recorded with a 4 mm MAS probe with a spinning rate of 4 kHz and contact time of 1 ms. Chemical shifts were referenced to tetramethylsilane (TMS) for ^{29}Si and adamantane for ^{13}C. FTIR spectra were recorded using a Nicolet Magna FTIR spectrometer with a narrow band MCT detector (Specac Ltd., London). Spectra were obtained from 128 scans with a 4 cm^{-1} resolution. High Resolution Scanning electron microscopy images (HR-SEM) were taken with Verios 460 (FEI) at a landing voltage of 0.5 kV in deceleration mode (stage bias voltage: 5 kV. The samples were mounted without metal coating (KAIST, Daejeon, Republic of Korea). The low-angle powder X-ray diffraction (XRD) patterns were obtained on a Rigaku Multiplex instrument operated at 2 kW using Cu Kα radiation (KAIST, Daejeon, Republic of Korea). XRD scanning was performed under ambient conditions in steps of 0.01, with an accumulation time of 0.5 s. Elemental analysis was performed by the combustion method using CHNS Analyzer Flash 2000, Thermo Scientific.

Extraction of REEs

Batch extraction studies

The solution of REEs (Sc, Y, La, Ce, Pr, Nd, Sm, Eu, Gd, Tb, Dy, Ho, Er, Tm, Yb, Lu) and additional ions, such as Al, Fe, Th and U in HNO_3 (pH = 4) were prepared with the desired concentration, i.e., (1) for the K_d values determination: 15 µg L^{-1} for all the pure silica materials, SBA-16(100)-DGA and MCM-41-DGA, 30 µg L^{-1} for all the grafted SBA-15 materials; (2) for the kinetics test: 50 µg L^{-1} for all the materials tested (3) for the adsorption isotherms: from 30 to 1000 µg L^{-1} for all the materials tested and an additional concentration i.e., 1500 µg L^{-1}, was used for SBA-15(80)-DGA. For batch extraction studies, the solution/solid ratio was fixed to 500 (V/m). The samples (10 mg) were shaken for 1 min and left under static conditions for 30 min. Subsequently the supernatant was filtered through a 0.2 µm syringe filter. The initial and final concentration of all the elements was determined by ICP-MS/MS (model 8800, Agilent Technologies). The data presented are average of triplicates.

Dynamic extraction studies

25 mg of mesoporous sorbents were packed inside a 2 mL cartridge (Eichrom Technologies, USA) using the slurry packing technique described elsewhere[7b]. Prior to extraction test, each column was conditioned with a solution of HNO_3 (10 mL), pH = 4. The solution of REEs (50 µg L^{-1}) was passed through the column at a nominal flow rate of 1 mL min^{-1} using a peristaltic pump (Minipuls 3, Gilson, USA) and 7 mL fractions were collected and analyzed by ICP-MS/MS (model 8800, Agilent Technologies).

Sorbent reusability studies

25 mg of mesoporous sorbents were packed into a cartridge as mentioned previously. Prior to the loading of the REEs solution (50 µg L^{-1}; 7 mL), columns were conditioned with a solution of HNO_3 pH = 4 (14 mL). The retained elements were eluted from the column with 7 mL of 0.1 M solution of ammonium oxalate $(NH_4)_2C_2O_4$. Afterwards, the columns were washed with nanopure water (7 mL), reconditioned with nitric acid and used for the second extraction. The above-mentioned procedure was repeated 4 times.

Results and discussion

Synthesis and characterization of the materials

The post-synthesis modification of the selected mesoporous silica supports (i.e., SBA-15, SBA-16 and MCM-41) was performed with the appropriate ligand (DGA) according to a standard procedure in dry toluene under reflux conditions yielding the respective DGA-functionalized materials. The low angle XRD patterns of the pure silica supports show well-resolved diffraction peaks corresponding to the different mesostructures expected, which confirms the high quality of the synthesized supports[8,9,10] (Figure S1a, ESI). The highly ordered structure of the mesoporous sorbents was also well maintained after functionalization with the DGA ligand, as revealed by the XRD patterns presented in Figure S1b, ESI. Furthermore, high resolution scanning electron microscopy (HRSEM) analysis also confirms that the ordered pore structure of the post-functionalized materials remains essentially intact and easily accessible. Some representative HRSEM images of the DGA-modified materials are shown in Figure 1 and Figure S2, ESI. As it can be noticed, the shape of MCM-41 particles, which tend to be more spherical (see Figure 1a), differs from the typical elongated particles of the SBA-15 family (see Figure 1c, 1g). Additionally, the porosity of the different SBA-15 materials seems to be slightly more opened through the particle surface with increasing aging temperature from SBA-15(60)-DGA to SBA-15(130). Overall, the HRSEM images of the hybrid materials are consistent with an increase in pore size and a somewhat lower channel tortuosity, which occur for SBA-15 silicas synthesized with increasing aging temperature.

The sorption isotherms are presented in Figure 2 and Figure S3-S5 and the porosity and structural parameters derived from the low temperature sorption of N_2 are depicted in Table 1. For SBA-15 and SBA-16 families, pristine and modified samples both show a pronounced capillary condensation step in the relative pressure range between 0.4-0.85 P/P_0 with a well resolved hysteresis loop. Increasing the aging temperature of the SBA-15 materials caused an obvious shift of the hysteresis loop towards higher P/P_0 values, indicative of increased pore size. For instance, pristine SBA-15 materials aged at 60 °C possess much smaller pores, i.e., 5.3 nm, whereas its counterpart aged at 130 °C has almost twice larger pores, 10.1 nm. Changing the aging temperature visibly affects also the vertical size of the hysteresis loop, which is associated with increase of the pore volume for materials synthetized at higher aging temperatures (see Table 1).[11]

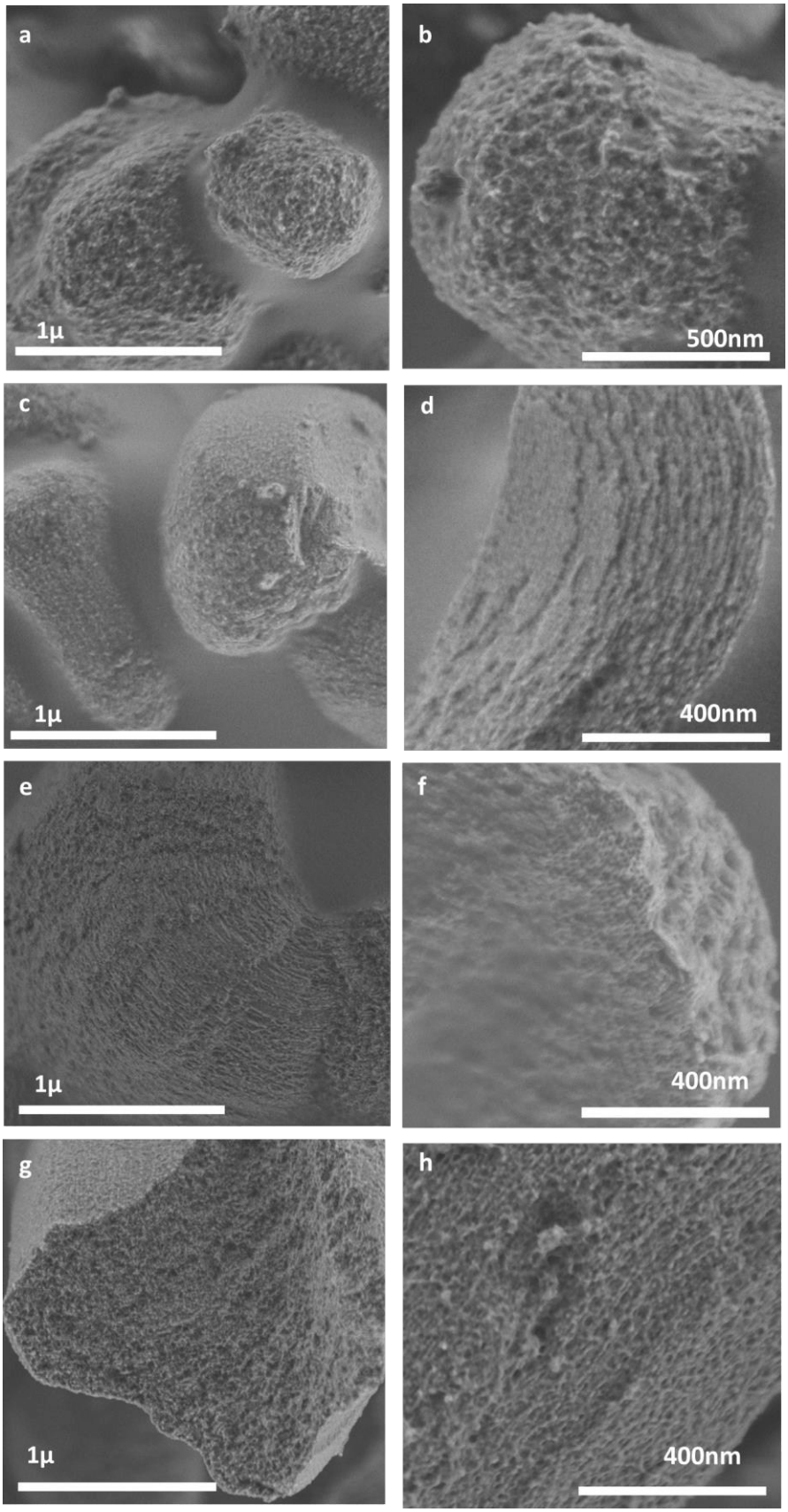

Figure 1: Representative HRSEM images of MCM-41-DGA (a, b), SBA-15(60)-DGA (c, d), SBA-15(100)-DGA (e, f) and SBA-15(130)-DGA (g, h).

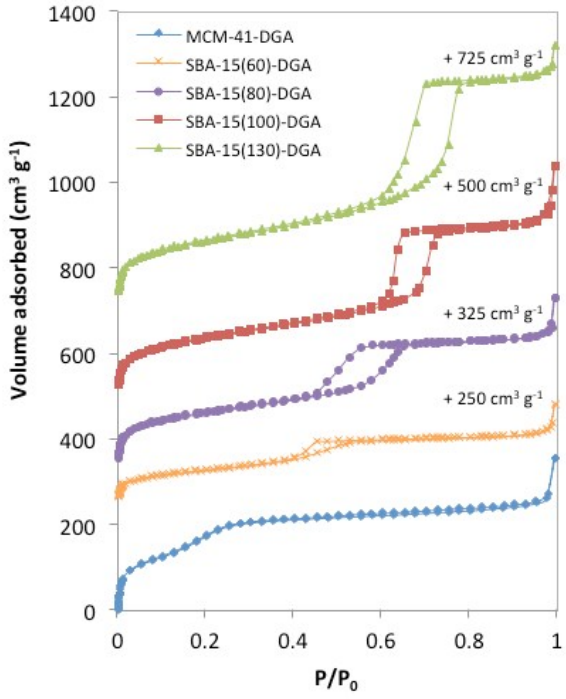

Figure 2: N_2 adsorption-desorption isotherms (-196°C) of the functionalized materials, as indicated.

For comparison purpose, Figure S3 shows also the isotherm of the MCM-41 material in which the pores are much smaller than SBA-15(60), being 4.1 nm, with the associated capillary condensation step occurring at lower relative pressure i.e., between 0.3-0.4 P/P_0. Furthermore, the pore sizes, specific surface area and pore volume for all materials have obviously diminished after the post-synthesis modification with the functional silane, demonstrating the efficiency of the mesopore functionalization. However, this decrease has not affected the quality of the materials since the shape of the hysteresis is still well maintained. Several analytical methods were used to characterize and confirm the covalent attachment of the DGA ligand (diglycol-2,4-diamido-propyltriethoxysilane) on the silica surface, such as solid state NMR and FTIR spectroscopies, CHN and thermogravimetric analysis. Since all the modified materials exhibit the same NMR profile, only a selected sample will be further described and presented in Figure 3. The ^{13}C CP/MAS NMR spectrum of SBA-15(80)-DGA material confirms the presence of the five carbon atoms existing in the DGA molecule. The formation of the amide bond can be confirmed by the peak at 171 ppm, which corresponds to the carbonyl atom in the amide group[14]. Further, carbon ether-type atoms are visible at 71 ppm[15]. The three remaining peaks are attributed to the CH_2 groups of the aminopropyl chain[14]. The absence of peaks at about 20 and 60 ppm suggests that there are no residual ethoxy groups or their concentration is relatively low[16]. Indeed, as shown on the ^{29}Si MAS NMR spectrum (Figure 3b), the DGA-ligand has been anchored to the silica support mostly through T^2 $(OH)(SiO)_2Si$-R and T^3 $(SiO)_3Si$-R species and the respective peaks are visible at -57 and -68 ppm[17]. As a consequence, the chemical attachment of the ligand through 2 or 3 chemical bonds makes it less likely to be leached from the surface upon the extraction procedure and may force a higher degree of rigidity than for adsorbed ligands used in commercial resins[18]. The presence of the amide bond on the surface of the sorbents was also confirmed by the presence of the amide I (1550 cm^{-1}) and amide II (1650 cm^{-1}) peaks[19] in the FTIR studies (Figure S6, ESI). Additionally, thermogravimetric analysis (TGA) was used to evaluate the efficiency of the grafting procedure. The amount of DGA ligand grafted on materials with various structures, e.g., SBA-16(100)-DGA, MCM-41-DGA and SBA-15(100)-DGA or samples with different pore size, e.g., SBA-15(60, 80, 100 or 130), and the corresponding mass loss profiles are presented in Table 1 and Figure S7, ESI respectively. In order to investigate the effect of the support structure, i.e., 3D pores SBA-16, large 2D pores SBA-15 and small 2D pores MCM-41 materials, on the extraction of REEs, the amount of ligand introduced for each grafting was kept equal, being around 20

Table 1: Physicochemical parameters of the pure and the functionalized silica materials; [a]calculated from TG analysis (air flow of 40 mL min^{-1}) from 150-650°C

Sample	S_{BET} (m^2 g^{-1})	V_{pore} (cm^3 g^{-1})	Pore size (nm)	Organic content[a] (%)	Decomposition T Air flow 20 mL min^{-1} (°C)	Decomposition T Air flow 40 mL min^{-1} (°C)
SBA-16(100)	1025	0.75	9.4	-	-	-
SBA-16(100)-DGA	387	0.33	8.8	18	340	340
MCM-41	1005	0.85	4.1	-	-	-
MCM-41-DGA	660	0.38	3.2	22	297, 336	277, 329
SBA-15(60)	633	0.61	5.3	-	-	-
SBA-15(60)-DGA	280	0.25	4.9	22	288, 336	330
SBA-15(80)	914	0.93	6.8	-	-	-
SBA-15(80)-DGA	492	0.48	5.7	23	290, 340	-
SBA-15(100)	825	1.16	8.5	-	-	-
SBA-15(100)-DGA	388	0.51	6.6	21	287, 335	325
SBA-15(130)	713	1.50	10.1	-	-	-
SBA-15(130)-DGA	505	0.81	8.2	22	258, 332	-

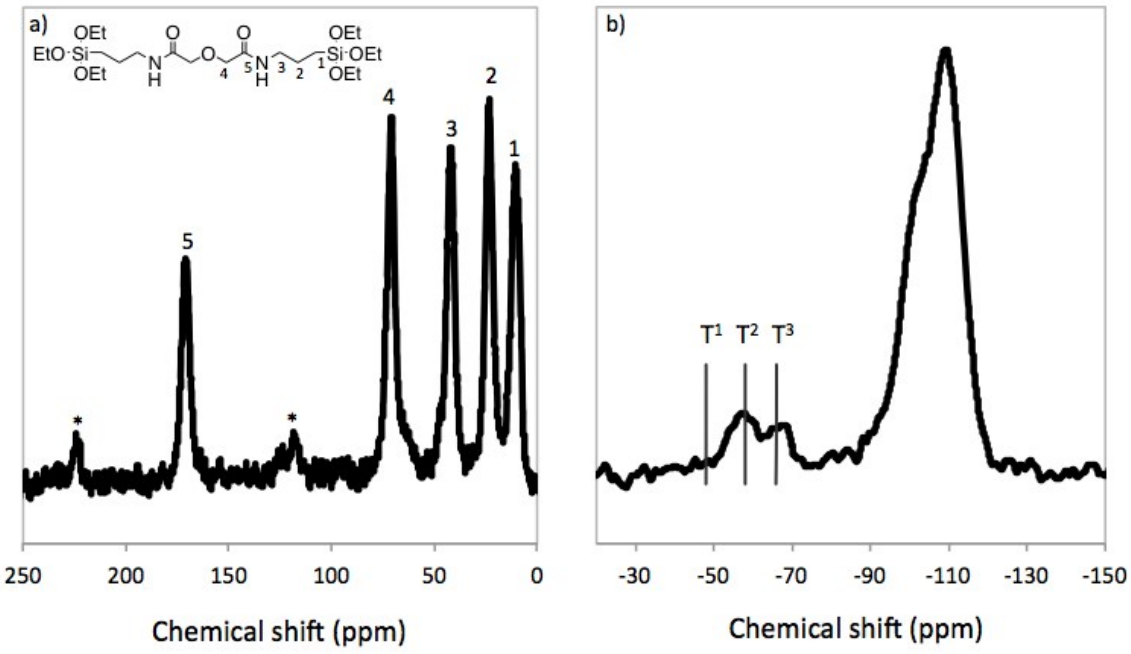

Figure 3: Solid state NMR of SBA-15(80)-DGA of a) ^{13}C CP/MAS and b) ^{29}Si MAS NMR spectra; *spinning side-bands of the carbonyl (5)

wt%, based on the TGA data (see Table 1). As confirmed by the CHN analysis (see Table S1, ESI), the targeted loading has been achieved for all materials with only small variation of the ligand content. Slightly lower amount of the ligand was observed for the SBA-16(100)-DGA material, even though the same quantity of modified silane was used in the modification step. This small difference in the amount of grafted ligand may be attributed to varying amounts of silanol groups in the different materials. The DSC profiles of selected DGA-functionalized materials, in the range of 200°C-600°C, are presented in Figure S8, ESI and the corresponding maximum decomposition temperatures (peak maxima) are listed in Table 1. The profiles of the thermal decomposition of the modified materials with the air flow 20 mL min^{-1} revealed that all the samples follow a two-step degradation. For MCM-41- and SBA-15-based systems, a lower temperature decomposition (exothermic effect) can be observed at about 290 °C while the second occurred at higher temperatures, above 330 °C (Figure S8a). The highest decomposition temperature of the DGA ligand, i.e., 340 °C, was observed for the SBA-16(100)-DGA sorbent, possibly as a result of a lower diffusivity of oxygen inside the cage-like pores and/or poorer diffusion of the decomposition products out of the material. In addition to this main decomposition peak at 340°C, this sample also shows a secondary effect appearing as a weak shoulder at about 410°C. To verify the influence of the air flow on the decomposition profiles, the measurements were also performed at a higher flow (40 mL min^{-1}). As seen from Figure S8b, except for the MCM-41-DGA sample, the decomposition of the samples occurred in one-step with a narrower peak. This observation could agree with a reduced oxygen accessibility or diffusion limitations occurring inside the smaller pore hybrid systems or pore-blocked SBA-16. Interestingly, similar to our previous results[7b], the increasing of the aging temperature, and therefore enlarging the pore size of SBA-15 material, shifts the decomposition temperature to the lower temperature range, i.e., 325 °C for SBA-15(100)-DGA vs. 330 °C for SBA-15(60)-DGA material (with air flow of 40 mL min^{-1}).

Batch extraction analysis

Extraction of REEs with and without competitive elements

The extraction behavior of our materials was first evaluated from the batch extraction system and the results, depicted as the distribution coefficient K_d (mL g^{-1})[20], are presented in Figure 4a and Figure S9, ESI. Clearly, functionalization with the DGA ligand significantly enhances the sorption capacity of the materials in comparison to the pure silica material. For instance, the K_d values for all un-functionalized silica supports exhibited very low lanthanides (Ln) uptake, 75 times lower than in case of the functionalized SBA-15(100) sorbent. Among different structures of the DGA-modified materials, SBA-16(100)-DGA sorbent shows the lowest Ln uptake, even if this material possesses comparable amount of the ligand grafted (Table 1). As such, this behavior highlights the importance of using a support with well-ordered and open porosity that provides an easy access to the ligand centers, on the extraction properties of sorbents. Further, it can be suggested that the porosity features primarily drive extraction capacity of the material and the ligand content is only secondary of importance. It is well documented that the structure of cage-like SBA-16 material is more likely to pore blocking, due to the presence of the narrow pore windows[7b,13,21]. Once the ligand is grafted on the SBA-16 support, the ink-bottle pores might be

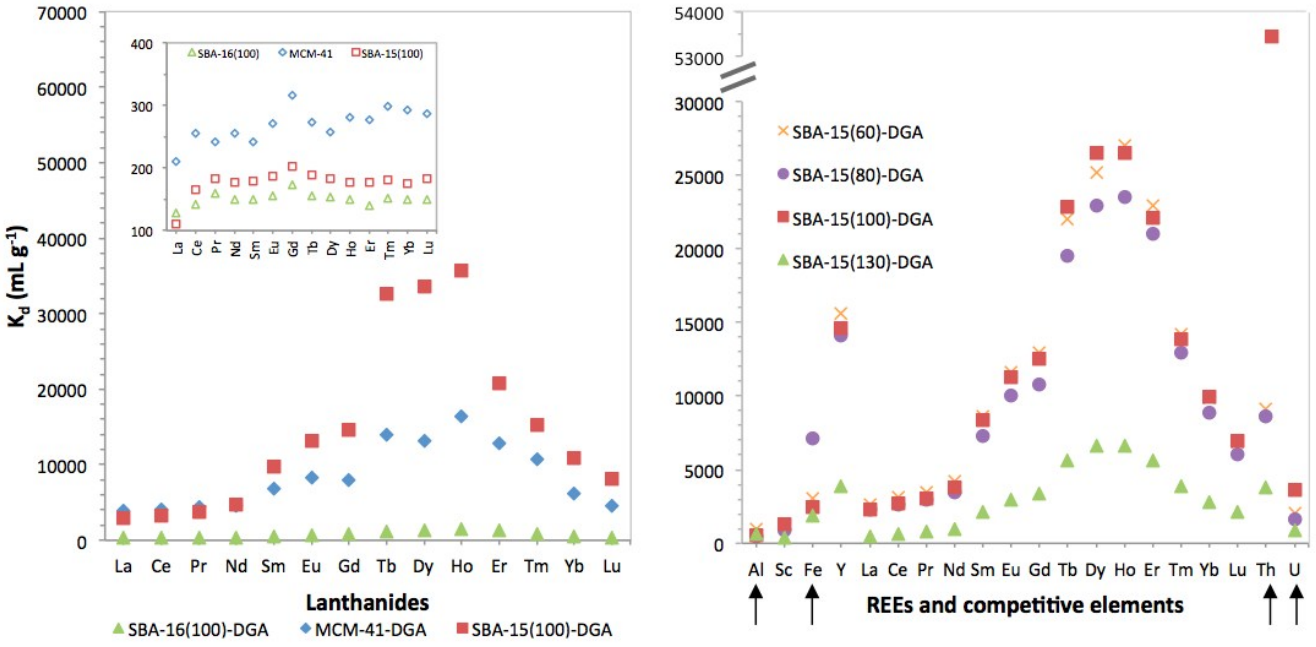

Figure 4: a) Ln extraction (K_d) of the pure and the functionalized materials with various morphologies; b) REEs and competitive elements (Al, Fe, Th and U) extraction of the functionalized SBA-15 materials with various pore sizes.

partially blocked and pore entrances can be significantly reduced thus hampering the accessibility to the ligand. This phenomenon will obviously be detrimental for the extraction capacity of the sorbent, like in the present case of SBA-16(100)-DGA material. Thus, the extraction behavior of this sorbent was not further investigated in details. Oppositely, the DGA-functionalized SBA-15 sorbents showed higher Ln uptake with a good selectivity towards the middle-size Ln, i.e., from Tb to Ho. Furthermore, as it can be observed in Figure 4b, Y^{3+} is also one of the preferentially extracted elements, for instance K_d values in the range 13000-17000 mL g^{-1} have been recorded for the SBA-15(60, 80, 100)-DGA materials. Interestingly, the ionic radii of the cations Tb^{3+}, Dy^{3+}, Ho^{3+}, i.e., 92.3, 90.8 and 89.4 pm, being the most efficiently extracted elements, are quite similar to Y^{3+}, being 89.2 pm[22]. Thus, the bite angle of the DGA ligand anchored into the SBA-15 materials could favor the capture of the cations with ionic size of approximately 90 pm[23]. Almost twice higher uptake of the mid-Ln has been observed for the large pore SBA-15(100)-DGA sorbent than for its smaller counterpart, which again signifies the role of the pore structure of the silica support on the extraction performance of materials. Though, the smaller pores of the MCM-41-DGA sorbent (3.2 nm) still provide interesting extraction environment with K_d values up to 16000 mL g^{-1} approximately.

Furthermore, the effect of the pore size on the extraction behavior of the silica sorbents was tested in case of SBA-15 materials aged at different temperatures. As shown in Figure S9, ESI, the lowest K_d values were obtained for the SBA-15(130)-DGA sorbent with the largest pore (8.2 nm), while SBA-15(60)-DGA (4.9 nm), SBA-15(80)-DGA (5.7 nm) and SBA-15(100)-DGA (6.6 nm) materials with smaller pores displayed much higher K_d, however, no significant difference was observed among the three other samples. Regarding these observations, confinement into smaller pores seems to enhance the extraction of the elements more than using a sorbent with much bigger pores, i.e., with pores above 8 nm. Interestingly, SBA-16-DGA, which also exhibited lower extraction capabilities, possesses as well pores larger than 7 nm.

Considering the fact that natural occurring REEs ores usually contain, in addition to REEs, significant amounts of other metals, such as trivalent elements (e.g., Al and Fe) and naturally-occurring radioelements (e.g., Th and U); we performed our batch extraction studies in the presence of these elements and the results are presented in Figure 4b. Interestingly, our materials showed low extraction capacities for the competing elements, being well below the K_d values observed for the targeted elements. For instance, the K_d values found for the middle size Ln, from Tb to Ho were approximately 19600 mL g^{-1} in average for the four materials tested, which is 9 times higher than the average K_d values found for the additional elements Al, Fe and U, being about 2100 mL g^{-1}. This behavior is especially well marked for the SBA-15 materials aged at 60, 80 and 100°C. For example, comparing the K_d values obtained for the most extracted element, Ho, (around 25700 mL g^{-1}), for these three materials, much lower average distribution coefficients were detected for Al, Fe and U, being around 660, 4300, 2500 mL g^{-1}, respectively. Therefore, the separation factors (SF)[24] between Ho and competing elements, expressed as the ratio between the respective K_d values, are 40 for Ho/Al, 6 for Ho/Fe and 11 for Ho/U, which makes the DGA-silica sorbents a very attractive alternative for the standard LLE purification/extraction methods. On the other hand, Th seems to be more difficult to separate from REEs in the one-step

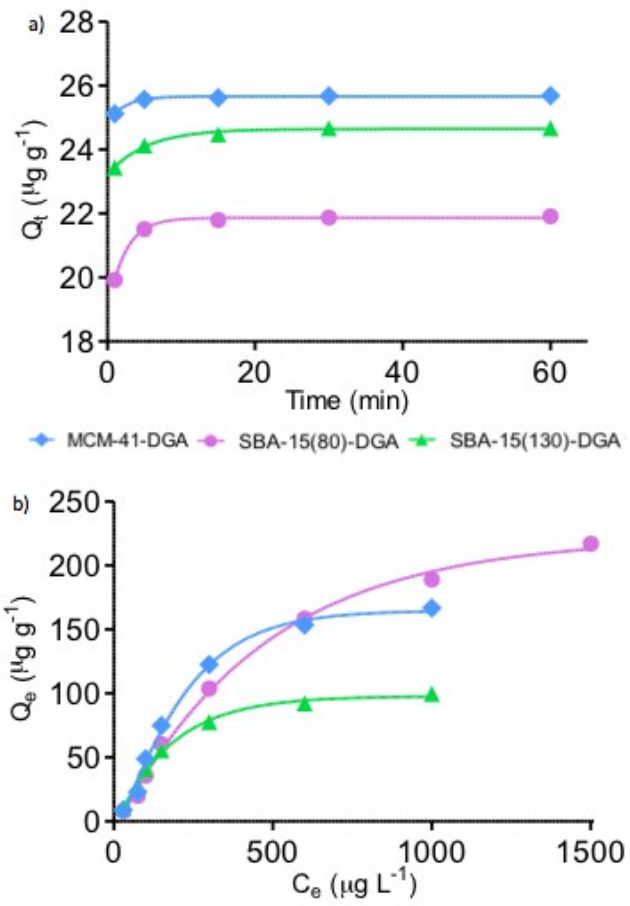

Figure 5: a) Kinetic curves fitted with the pseudo-second-order; b) Adsorption isotherms fitted with the Langmuir model.

extraction, although, the SF Ho/Th is still above 3 for SBA-15(60)-DGA, SBA-15(80)-DGA and SBA-15(130)-DGA. However, unexpectedly high K_d value was found for the extraction of Th with SBA-15(100)-DGA. As the ionic radius of Th resembles the one of Ho in comparison to Al and Fe which are much smaller cations, it is possible that the spatial arrangement of DGA ligands grafted on the silica surface in SBA-15(100)-DGA is optimal for Th extraction. Further investigations need to be performed on this particular aspect in order to confirm this peculiar behavior of Th.

Kinetics studies

In order to determine whether the different textural properties of the silica sorbents influence the rate of REEs adsorption, kinetic studies were performed and the corresponding results are presented in Figure 5a as a function of the average amount of adsorbed metal Q_t vs. time. In this study, we kept the same pH of the extraction solution (HNO_3, pH = 4), however, we increased the initial concentration of REEs solution up to 50 μg L^{-1} (see the experimental part for the details) and varied the extraction time from 1 to 60 minutes.

As shown, the adsorption equilibrium for all materials is reached within only few minutes despite the different pore structures and morphology of the sorbents, i.e., around 5 minutes, which is much shorter than results reported in the literature[25]. All materials tested show a similar adsorption profile with comparable amount of adsorbed metal ions, i.e., Q_t = 22, 25, 26 mg g^{-1} for SBA-15(80)-DGA, SBA-15(130)-DGA and MCM-41-DGA respectively. Different kinetic models, i.e. pseudo-first-order, pseudo-second-order models were applied to the data (Figure 5a) in order to investigate the controlling mechanism of the sorption process[26]. The theoretical values of the sorption capacity were calculated from the slopes and intercepts of the corresponding plots and relevant kinetics parameters are shown in Table S2 and Figure S10. Considering the r^2 values obtained for all materials, the pseudo-second-order model fits the best to our experimental data. Such model suggests that the adsorption of REEs with our sorbents can be described as a chemisorption process, driven by electron exchange between the targeted elements and the host materials[27].

Adsorption isotherms

In order to determine whether the morphology or the pore size have an effect on the extraction capacity of different silica supports, adsorption isotherms were performed and the results are presented in Figure 5b. In this experiment, the initial concentration of REEs was varied in a broad range, i.e., from 30 to 1500 μg mL^{-1}, while other parameters were kept constant (see experimental part for the details). The linear regression of both models can be found in Figure S11 and the parameters corresponding to these models are presented in Table S2, ESI. From the r^2 values reported in Table S2, it is obvious that the Langmuir model of adsorption fits better with our experimental results than the Freundlich model[28]. It can be easy noticed from our results that despite the same functionalization of all sorbents the materials possess different maximum extraction capacity and the highest REEs uptake was observed for the SBA-15(80)-DGA sample (approximately 200 μg g^{-1}). Moreover, these three sorbents showed significant differences in the amount of REEs adsorbed. These results support our previous assumption that sorbents with smaller pore (i.e., 3.2 nm and 5.7 nm for MCM-41-DGA and SBA-15(80)-DGA) improved the REEs uptake, in comparison to the big-pore material (i.e., 8.2 nm for SBA-15(130)-DGA), most likely owing to the more favorable ligand geometry in smaller pores. Furthermore, it should be kept in mind that the observed Q_{max} values are calculated from the mixture of 17 elements not only from the single-element solutions, which may implicate that the observed maximum sorption capacity for the single metal extraction may be higher.

Dynamic extraction of REEs and reusability of the mesoporous sorbents

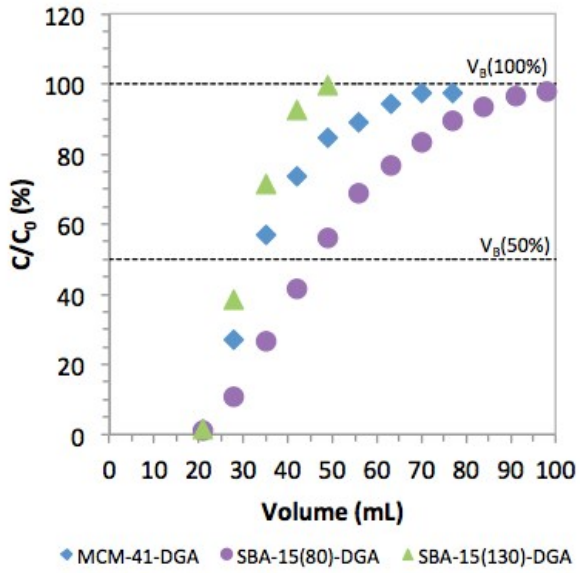

Figure 6: Breakthrough curves derived from the dynamic extraction of REEs.

Although, the results from the batch extraction system proved the good performance of our hybrid sorbents, they need to be supplemented by evaluation of the actual performances of these materials in flow through conditions similar to those used in the industrial setups. Therefore, we tested the synthesized materials under flow through conditions.

The results are presented as the breakthrough curves in Figure 6. The sigmoidal breakthrough curves draw the percentage of the un-retained elements as a function of the volume of extraction solution. These curves further help to determine the breakthrough volume of the system (V_B) which directly corresponds to the amount of elements eluted upon continuous loading of REEs solution, in other words, V_B describes the saturation point of the sorbent in the dynamic conditions[7b]. Therefore, the higher V_B value means better retention capacity of the sorbent.

In our studies, the initial concentration of the mixed REEs was fixed to 50 µg L^{-1}. According to the results presented in Figure 6, $V_{B,50\%}$ is equal to 29, 32 and 49 mL for SBA-15(130)-DGA, MCM-41-DGA and SBA-15(80)-DGA respectively. As it can be seen from the Figure 6, the volume $V_{100\%}$ corresponding to the saturation of the materials is approximately 49, 77 and 98 mL for SBA-15(130)-DGA, MCM-41-DGA and SBA-15(80)-DGA respectively. These volumes are considerable if compared to the quantities of solid materials used in this experiment (25 mg). The SBA-15(130)-DGA material, with large pore (8.2 nm), reach the saturation level after passing through the column approximately half of the volume of REEs solution needed to saturate SBA-15(80)-DGA sorbent (5.7 nm). The volume $V_{100\%}$ of the sample MCM-41-DGA is closer to one observed for SBA-15(80)-DGA, confirming the trend observed previously in the K_d determination or in the adsorption isotherm study for instance. Additionally, SBA-15-based mesoporous sorbents can be regarded as very stable sorbents for REEs separation. As presented in Figure 7, the materials can be used in at least four extraction-release cycles without any significant loss in the extraction performance. Likewise, the porosity of these sorbents has been successfully preserved after the four extraction cycles (Figure S12, ESI). However, it can be observed in the case of MCM-41-DGA that the isotherm shifts to higher volume of N_2 adsorbed, indicating that few percent of the ligand might have been detached from the surface which is not as pronounced for SBA-15(80)-DGA.

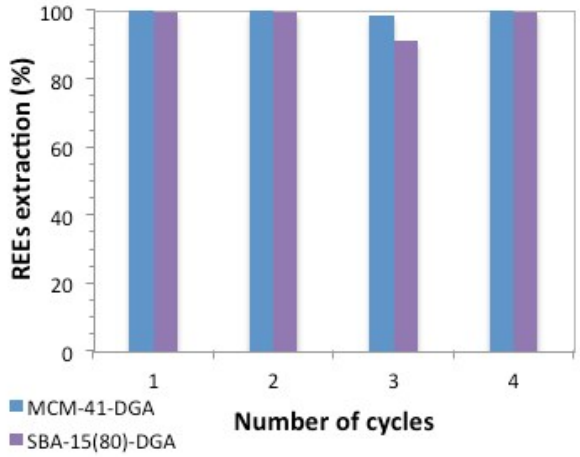

Figure 7: Reusability of MCM-41-DGA (left) and SBA-15(80)-DGA (right) over 4 cycles of REEs extraction.

Conclusion

Our work aimed at exploring more deeply the role of the pore structure, texture and morphology of the DGA-functionalized mesoporous silica materials on their REEs adsorption performances. From our results, the 2D hexagonal structure appears more advantageous than the 3D cage-like structure; the shape and narrow connectivity of the pores in SBA-16 materials seem more prone to pore blocking and therefore lead to a reduced accessibility to the coordinating sites of the DGA ligand. On the other hand, the SBA-15 materials with smaller pore i.e., aged at lower temperature (below 100°C) seem to provide a certain confinement and therefore enhance the REEs adsorption. Indeed, we observed the highest capacity of extraction in both static and dynamic conditions for the SBA-15(80)-DGA (5.2 nm) compared to its bigger pore equivalent SBA-15(130)-DGA (8.2 nm). These findings provide insights into the surface chemistry and porosity contributions of the functionalized solid supports in order to further improve the material design, both in the batch and dynamic systems.

Acknowledgement

The authors wish to acknowledge Fonds de Recherche Québecois Nature et Technologies (FRQNT) and National Sciences and Engineering Research Council of Canada (NSERC) for the financial support. The Natural Sciences and Research Council of Canada through a Strategic Project Grant supported this work. The authors also thank Prof. R. Ryoo and Mun-Hee (KAIST and Institute for Basic Science, Daejeon, Republic of Korea) for providing the low angle powder XRD data.

Notes and references

1 United States Environmental Protection Agency, Rare Earth Elements: A Review of Production, Processing, Recycling and Associated Environmental Issues, 2012.
2 K. Binnemans, P. T. Jones, B. Blanpain, T. Van Gerven, Y. Yang, A. Walton, M. Buchert, *J. Clean. Prod.*, 2013, **51**, 1.
3 D. J. Hanson, *Chem. Eng. News*, 2011, **89**, 28.
4 (a) S. Massari, M. Ruberti, *Res. Policy*, 2013, **38**, 36; (b) K. Binnemans, P. T. Jones, *J. Rare Earths*, 2014, **32**, 195.
5 C. K. Gupta, N. Krishnamurthy, Extractive Metallurgy of Rare Earths, 2005, CRC Press.
6 (a) V. N. Epov, K. Benkhedda, R. J. Cornett, R. D. Evans, *J. Anal. At. Spectrom.*, 2005, **20**, 424; (b) D. Larivière, T. A. Cumming, S. Kiser, C. Li, R. J. Cornett, *J. Anal. At. Spectrom.*, 2008, **23**, 352.
7 (a) P. J. Lebed, K. de Souza, F. Bilodeau, D. Larivière, F. Kleitz, *Chem. Commun.*, 2011, **47**, 11525; (b) P. J. Lebed, J. -D Savoie, J. Florek, F. Bilodeau, D. Larivière, F. Kleitz, *Chem. Mater.*, 2012, **24**, 4166; (c) J. Florek, F. Chalifour, F. Bilodeau, D. Larivière, F. Kleitz, *Adv. Funct. Mater.*, 2014, **24**, 2668.
8 M. Choi, W. Heo, F. Kleitz, R. Ryoo, *Chem. Commun.*, 2003, **75**, 1340.
9 F. Kleitz, T. -W. Kim, R. Ryoo, *Langmuir*, 2006, **22**, 440.
10 F. Kleitz, W. Schmidt, F. Schüth, *Microporous Mesoporous Mater.*, 2003, **65**, 1.
11 (a) P. I. Ravikovitch, A. V. Neimark, *J. Phys. Chem. B*, 2001, **105**, 6817; (b) F. Kleitz, F. Bérubé, R. Guillet-Nicolas, C.-M. Yang, M. Thommes, *J. Phys. Chem. C* 2010, **114**, 9344; (c) H. Staub, R. Guillet-Nicolas, N. Even, L. Kayser, F. Kleitz, F.-G. Fontaine, *Chem. Eur. J.* 2011, **17**, 4254.
12 (a) A. V. Neimark, *Stud. Surf. Sci. Catal.*, 1998, **117**, 77; (b) A. V. Neimark, P. I. Ravikovitch, M. Grün, F. Schüth, K. K. Unger, *J. Colloid Interface Sci.*, 1998, **207**, 159; (c) P. I. Ravikovitch, A. V. Neimark, *Stud. Surf. Sci. Catal.*, 2000, **129**, 597.
13 F. Kleitz, T. Czuryszkiewicz, L. A. Solovyov, M. Lindén, *Chem. Mater.*, 2006, **18**, 5070.
14 H. S. Park, C. W. Kim, H. J. Lee, J. H. Choi, S. G. Lee, Y. –P. Yun, I. C. Kwon, S. J. Lee, S. Y. Jeong, S. C. Lee, *Nanotechnology*, 2010, **21**, 225101.
15 S. Antonijevic, N. Halpern-Manners, *Solid State Nucl. Mag. Res.*, 2008, **33**, 82.
16 J. Blüemel, *J. Am. Chem. Soc.*, 1995, **117**, 2112.
17 (a) M. Lelli, D. Gajan, A. Lesage, M. A. Caporini, V. Vitzthum, P. Miéville, F. Héroguel, F. Rascón, A. Roussey, C. Thieuleux, M. Boualleg, L. Veyre, G. Bodenhausen, C. Copéret, L. Emsley, *J. Am. Chem. Soc.*, 2011, **133**, 2104; (b) A. S. Maria Chong, X. S. Zhao, *J. Phys. Phys. Chem.*, 2003, **107**, 12650.
18 Z. Wu, D. Zhao, *Chem. Commun.*, 2011, **47**, 3332.
19 D. Lunn, D. F. Shantz, *Chem. Mater.*, 2009, **21**, 3638.
20 G. E. Fryxell, H. Wu, Y. Lin, W. J. Shaw, J. C. Birnbaum, J. C. Linehan, Z. Nie, K. Kemner, S. Kelly, *J. Mater. Chem.*, 2004, **14**, 3356.
21 P. I. Ravikovitch, A. V. Neimark, *Langmuir*, 2002, **18**, 9830.
22 I. McGill, Rare Earth Elements, Ullmann's Encyclopedia of Industrial Chemistry, 2012, Wiley-VCH, Weinheim.
23 J. Florek, A. Mushtaq, D. Larivière, G. Cantin, F.-G. Fontaine, F. Kleitz, *RSC Adv.*, 2015, **5**, 103782.
24 D. G. Kalina, E. P. Horwitz, L. Kaplan, A. C. Muscatello, *Separ. Sci. Technol.,* 1981, **16**, 1127.
25 (a) M. R. Awual, M. M. Hasan, M. Naushad, H. Shiwaku, T. Yaita, Chem. Eng. J., 2015, 265, 210; (b) L. Zuo, S. Yu, H. Zhou, J. Jiang, X. Tian, *J. Radioanal. Nucl. Chem.*, 2011, **288**, 579.
26 N. Chiron, R. Guilet, E. Drydier, *Water Res.,* 2003, **37**, 3079.
27 Y. S. Ho, *J. Hazard. Mater.*, 2006, **B136**, 681.
28 K. Y. Foo, B. H. Hameed, *Chem. Eng. J.,* 2010, **156**, 2.

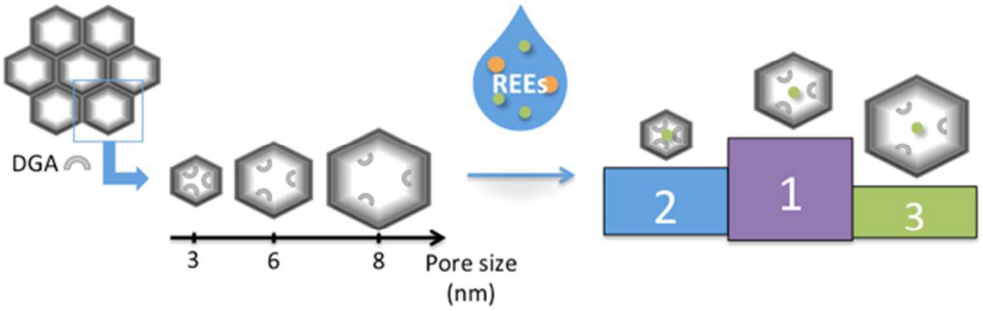

225x75mm (72 x 72 DPI)